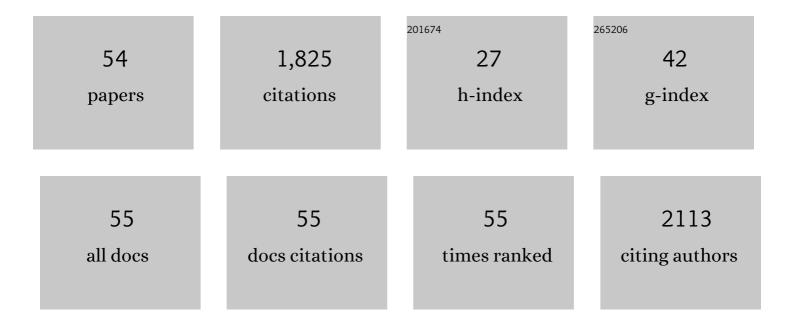
Tao Yang

List of Publications by Year in descending order

Source: https://exaly.com/author-pdf/2415190/publications.pdf Version: 2024-02-01



#	Article	IF	CITATIONS
1	Superior Photodetectors Based on All-Inorganic Perovskite CsPbI ₃ Nanorods with Ultrafast Response and High Stability. ACS Nano, 2018, 12, 1611-1617.	14.6	210
2	Piezoelectric Nanogenerator Based on In Situ Growth Allâ€Inorganic CsPbBr ₃ Perovskite Nanocrystals in PVDF Fibers with Longâ€Term Stability. Advanced Functional Materials, 2021, 31, 2011073.	14.9	95
3	Electrochemical detection mechanism of dopamine and uric acid on titanium nitride-reduced graphene oxide composite with and without ascorbic acid. Sensors and Actuators B: Chemical, 2019, 298, 126872.	7.8	92
4	B-doped 3C-SiC nanowires with a finned microstructure for efficient visible light-driven photocatalytic hydrogen production. Nanoscale, 2015, 7, 8955-8961.	5.6	80
5	In situ reduced MXene/AuNPs composite toward enhanced charging/discharging and specific capacitance. Journal of Advanced Ceramics, 2021, 10, 1061-1071.	17.4	78
6	Improved microwave absorption performance of modified SiC in the 2–18 GHz frequency range. CrystEngComm, 2017, 19, 519-527.	2.6	63
7	Preparation of Zr ⁴⁺ doped calcium hexaaluminate with improved slag penetration resistance. Journal of the American Ceramic Society, 2021, 104, 4854-4866.	3.8	61
8	Ultra-Stable and Durable Piezoelectric Nanogenerator with All-Weather Service Capability Based on NÂDoped 4H-SiC Nanohole Arrays. Nano-Micro Letters, 2022, 14, 30.	27.0	57
9	The oxidation and thermal stability of two-dimensional transition metal carbides and/or carbonitrides (MXenes) and the improvement based on their surface state. Inorganic Chemistry Frontiers, 2021, 8, 2164-2182.	6.0	56
10	Piezoelectric nanogenerators with high performance against harsh conditions based on tunable N doped 4H-SiC nanowire arrays. Nano Energy, 2021, 83, 105826.	16.0	56
11	Tunable preparation of chrysanthemum-like titanium nitride as flexible electrode materials for ultrafast-charging/discharging and excellent stable supercapacitors. Journal of Power Sources, 2018, 396, 319-326.	7.8	54
12	Highâ€Performance SiC Nanobelt Photodetectors with Longâ€Term Stability Against 300 °C up to 180 Days. Advanced Functional Materials, 2019, 29, 1806250.	14.9	54
13	Porous hexagonal boron nitride whiskers fabricated at low temperature for effective removal of organic pollutants from water. Ceramics International, 2016, 42, 8754-8762.	4.8	53
14	A Facile Synthesis of a Three-Dimensional Flexible 3C-SiC Sponge and Its Wettability. Crystal Growth and Design, 2014, 14, 4624-4630.	3.0	48
15	Electrostatic interaction assisted synthesis of a CdS/BCN heterostructure with enhanced photocatalytic effects. Journal of Materials Chemistry C, 2020, 8, 1803-1810.	5.5	48
16	Preparation of TiO _x N _y /TiN composites for photocatalytic hydrogen evolution under visible light. Physical Chemistry Chemical Physics, 2015, 17, 28782-28788.	2.8	47
17	Photodetectors with ultra-high detectivity based on stabilized all-inorganic perovskite CsPb _{0.922} Sn _{0.078} 1 ₃ nanobelts. Journal of Materials Chemistry C, 2018, 6, 6287-6296.	5.5	47
18	Cadmium sulfide with tunable morphologies: Preparation and visible-light driven photocatalytic performance. Physica E: Low-Dimensional Systems and Nanostructures, 2017, 93, 116-123.	2.7	45

Tao Yang

#	Article	IF	CITATIONS
19	Construction of layered h-BN/TiO2 hetero-structure and probing of the synergetic photocatalytic effect. Science China Materials, 2020, 63, 276-287.	6.3	39
20	Mild fabrication of SiC/C nanosheets with prolonged cycling stability as supercapacitor. Journal of Materials Science and Technology, 2022, 110, 178-186.	10.7	39
21	TiN @NiCo2O4 coaxial nanowires as supercapacitor electrode materials with improved electrochemical and wide-temperature performance. Journal of Alloys and Compounds, 2017, 692, 605-613.	5.5	37
22	Bare and boron-doped cubic silicon carbide nanowires for electrochemical detection of nitrite sensitively. Scientific Reports, 2016, 6, 24872.	3.3	34
23	Single crystalline 3C-SiC whiskers used for electrochemical detection of nitrite under neutral condition. Ionics, 2016, 22, 1493-1500.	2.4	34
24	Synergizing the multiple plasmon resonance coupling and quantum effects to obtain enhanced SERS and PEC performance simultaneously on a noble metal–semiconductor substrate. Nanoscale, 2017, 9, 2376-2384.	5.6	33
25	Ti ₃ C ₂ T _{<i>x</i>} (MXene)/Pt nanoparticle electrode for the accurate detection of DA coexisting with AA and UA. Dalton Transactions, 2022, 51, 4549-4559.	3.3	33
26	Enhancing photoluminescence properties of SiC/SiO ₂ coaxial nanocables by making oxygen vacancies. Dalton Transactions, 2016, 45, 13503-13508.	3.3	32
27	Preparation of hexagonal BN whiskers synthesized at low temperature and their application in fabricating an electrochemical nitrite sensor. RSC Advances, 2016, 6, 27767-27774.	3.6	31
28	The effective determination of Cd(<scp>ii</scp>) and Pb(<scp>ii</scp>) simultaneously based on an aluminum silicon carbide-reduced graphene oxide nanocomposite electrode. Analyst, The, 2017, 142, 2741-2747.	3.5	28
29	Tunable fabrication of single-crystalline CsPbI3 nanobelts and their application as photodetectors. International Journal of Minerals, Metallurgy and Materials, 2021, 28, 1030-1037.	4.9	26
30	Individual and Simultaneous Voltammetric Determination of Cd(II), Cu(II) and Pb(II) Applying Amino Functionalized Fe ₃ O ₄ @Carbon Microspheres Modified Electrode. Electroanalysis, 2019, 31, 1448-1457.	2.9	24
31	Supercapacitor electrode based on few-layer h-BNNSs/rGO composite for wide-temperature-range operation with robust stable cycling performance. International Journal of Minerals, Metallurgy and Materials, 2020, 27, 220-231.	4.9	24
32	Effect of temperature on the initial reaction behavior of MAB phases (MoAlB powders) at 700–1000°C in air. Ceramics International, 2021, 47, 20700-20705.	4.8	19
33	All-inorganic dual-phase halide perovskite nanorings. Nano Research, 2020, 13, 2994-3000.	10.4	18
34	Synthesis of titanium nitride nanopowder at low temperature from the combustion synthesized precursor and the thermal stability. Journal of Alloys and Compounds, 2014, 615, 838-842.	5.5	17
35	A wide range photoluminescence intensity-based temperature sensor developed with BN quantum dots and the photoluminescence mechanism. Sensors and Actuators B: Chemical, 2020, 304, 127353.	7.8	16
36	Template free synthesis of highly ordered mullite nanowhiskers with exceptional photoluminescence. Ceramics International, 2015, 41, 9560-9566.	4.8	13

Tao Yang

#	Article	IF	CITATIONS
37	Molten salt synthesis of mullite nanowhiskers using different silica sources. International Journal of Minerals, Metallurgy and Materials, 2015, 22, 884-891.	4.9	13
38	Fabrication of Ordered Mullite Nanowhisker Array with Surface Enhanced Raman Scattering Effect. Scientific Reports, 2015, 5, 9690.	3.3	10
39	Improvement in surface-enhanced Raman spectroscopy from cubic SiC semiconductor nanowhiskers by adjustment of energy levels. Physical Chemistry Chemical Physics, 2016, 18, 27572-27576.	2.8	9
40	Simultaneous determination of Cd(II) and Pb(II) using electrode modified by FeAl2O4-AlOOH-reduced graphene oxide hybrids. Ionics, 2019, 25, 2351-2360.	2.4	9
41	Pt-Co Alloys-Loaded Cubic SiC Electrode with Improved Photoelectrocatalysis Property. Materials, 2017, 10, 955.	2.9	8
42	New approach to evaluate the influence of compressive stress on the oxidation of non-oxide ceramics. Ceramics International, 2021, 48, 2317-2317.	4.8	7
43	Evidence of the enhanced negative thermal expansion in (1 â^' x)PbTiO3-xBi(Zn2/3Ta1/3)O3. Inorganic Chemistry Frontiers, 2020, 7, 1284-1288.	6.0	6
44	Strong Covalent Bonding for Enhanced Negative Thermal Expansion in (1 –) Tj ETQq0 0 0 rgBT /Overlock 10 Tr 20445-20449.	f 50 467 T 3.1	d (<i>x</i>)P 5
45	Recovery Behavior of Separating Britholite (Ca3Ce2[(Si,P)O4]3F) Phase from Rare-Earth-rich Slag by Centrifugal Casting. High Temperature Materials and Processes, 2015, 34, .	1.4	4
46	Tunable thermal expansion and high hardness of (0.9Ⱂ <i>x</i>)PbTiO ₃ – <i>x</i> CaTiO ₃ –0.1Bi(Zn _{2/3} Ta _{1/3Inorganic Chemistry Frontiers, 2019, 6, 1068-1072.}	ub <i>x</i>) .0 <su< td=""><td>b>34ce</td></su<>	b>34ce
47	Large nonlinear optical effect in tungsten bronze structures <i>via</i> Li/Na cross-substitutions. Chemical Communications, 2020, 56, 8384-8387.	4.1	3
48	Reply to "Comment on â€~Superior Photodetectors Based on All-Inorganic Perovskite CsPbI ₃ Nanorods with Ultrafast Response and High Stability'― ACS Nano, 2018, 12, 10571-10571.	14.6	2
49	Semi-empirical estimation for enhancing negative thermal expansion in PbTiO3-based perovskites. International Journal of Minerals, Metallurgy and Materials, 2022, 29, 783-786.	4.9	2
50	A novel immune image template set for fuzzy image segmentation and its application research. , 2011, , .		1
51	Manifold fitting algorithm of noisy manifold data based on variable-scale spectral graph. Soft Computing, 0, , 1.	3.6	1
52	Fabrication of Semiconductor with Modified Microstructure for Efficient Photocatalytic Hydrogen Evolution Under Visible Light. , 0, , .		0
53	A Manifold-Based Dimension Reduction Algorithm Framework for Noisy Data Using Graph Sampling and Spectral Graph. Complexity, 2020, 2020, 1-18.	1.6	0
54	A Projective Noise Reduction Algorithm Based on Laplacian Smoothing. , 2021, , .		0